Available online at www.sciencedirect.com
ScienceDirect
Journal of Volcanology and Geothermal Research 167 (2007) 37–56
Journal of volcanology and geothermal research
www.elsevier.com/locate/jvolgeores

Seismic tomography of magmatic systems

Jonathan M. Lees *

The University of North Carolina at Chapel Hill Department of Geological Sciences Campus Box #3315 Chapel Hill, NC 27599-3315, United States

Available online 8 August 2007

Abstract

Seismic inversion for three-dimensional variations of velocity and attenuation are often used to delineate magma bodies in the crust and upper mantle. Problems related to spatial resolution and data noise can obscure details relevant to investigating magma chambers, and the introduction of smoothing constraints, or damping, causes blurring. Tomographic inversions for P- and S-wave velocity/attenuation are summarized including large calderas, rift zones and smaller scale subduction zone volcanoes. While results vary considerably from place to place, most anomalies are found to be in the range of ±10% perturbation, a range often controlled by the method of smoothing or regularization imposed during analysis. At many volcanoes high velocity anomalies are observed in the shallow regions below active areas where conduits, dykes or sills are expected to be present. At other locations low velocity perturbations are seen and interpreted as magma accumulation. Resolution limitations and regularization play a significant role in determining the level of perturbation observed in tomographic studies, although there may be regions where diffuse accumulations of magma do not exhibit strong anomalies and their identification will be elusive.

Keywords: tomography; seismic velocity; attenuation; magma; magma chamber; melt accumulation

1. Introduction: What is tomography?

In this paper I review some of the basic methodology of tomographic inversion of seismic waves in a non-technical way, with the intent to reach a broad audience of non-specialists. There is general confusion about how this method is applied in seismic situations and often interpretation (or over interpretation) can be a problem. In many cases results are ambiguous and researchers seek explanations by invoking geological insight and *a priori* information as constraints. It is extremely important for readers and researchers, however, to emphasize the importance of the influence of incomplete and noisy data. These problems can only be overcome by raising the quality of data acquisition, data analysis and by increasing the total number and spatial distribution of seismic stations.

Tomography (literally, 'slice picture') originated in radio astronomy as a method to image aspects of remote regions of the universe. Later physicists and bio-physicists collaborated to create the first methodology and instrumentation that led to the first tomographic analysis of live tissue, especially human bodies. This approach was called "computer aided tomography" or CAT scans. Researchers who pioneered these methods received the Nobel Prize in physiology and medicine in 1979 (Allan Cormack and Godfrey Hounsfield). At the same time seismologists recognized that similar methodology could be applied to imaging the earth. Early papers on these approaches were not called tomography, but simply "three-dimensional

* Tel.: +919 962 0695; fax: +919 966 4519.
E-mail address: jonathan_lees@unc.edu.
URL: http://www.unc.edu/~leesj.

0377-0273/$ - see front matter © 2007 Published by Elsevier B.V.
doi:10.1016/j.jvolgeores.2007.06.008

analysis". It was not until the early 1980's that data sets large enough to actually mimic an approach similar to medical tomography emerged. An extensive collection of review papers about various aspects of tomographic analysis in seismology can be found in the compilation of Iyer and Hirahara (1993).

The basic idea is illustrated in cartoon form in Fig. 1. Earthquakes emit seismic energy that travels out to the stations at the surface. At first, we assume an intervening velocity structure, typically one dimensional, and use that to predict travel times to each station. If the model is correct the difference between predicted and observed arrivals will be small. If waves pass through anomalous structures, however, travel times will be perturbed and the differences will become significant. Seismic tomography often involves using the travel-time residuals to reconstruct anomalies where large numbers of raypaths overlap at varying angles. It can be shown that with complete coverage from all angles, the anomalous body can be reconstructed perfectly. This ideal situation is never achieved in real analyses, of course.

One main difference between medical tomography and seismic tomography is the simple fact that in the laboratory one can entirely surround the target body and thus get a complete, or nearly complete, view of the object studied. Under these conditions and geometries medical tomography can employ specially devised mathematical methods to perform the inversion, in particular the radon transform (the radon transform is a two dimensional integral, much like the Fourier transform, that allows one to convert line integrals of properties across a section into an image (Herman, 1980)). In local earthquake seismology this option is generally not available and other, more straightforward, methodologies (back-projection, for example) must be employed. Three dimensional seismic analysis usually invokes a very simple idea called "back-projection tomography". In this approach the difference between the predicted and

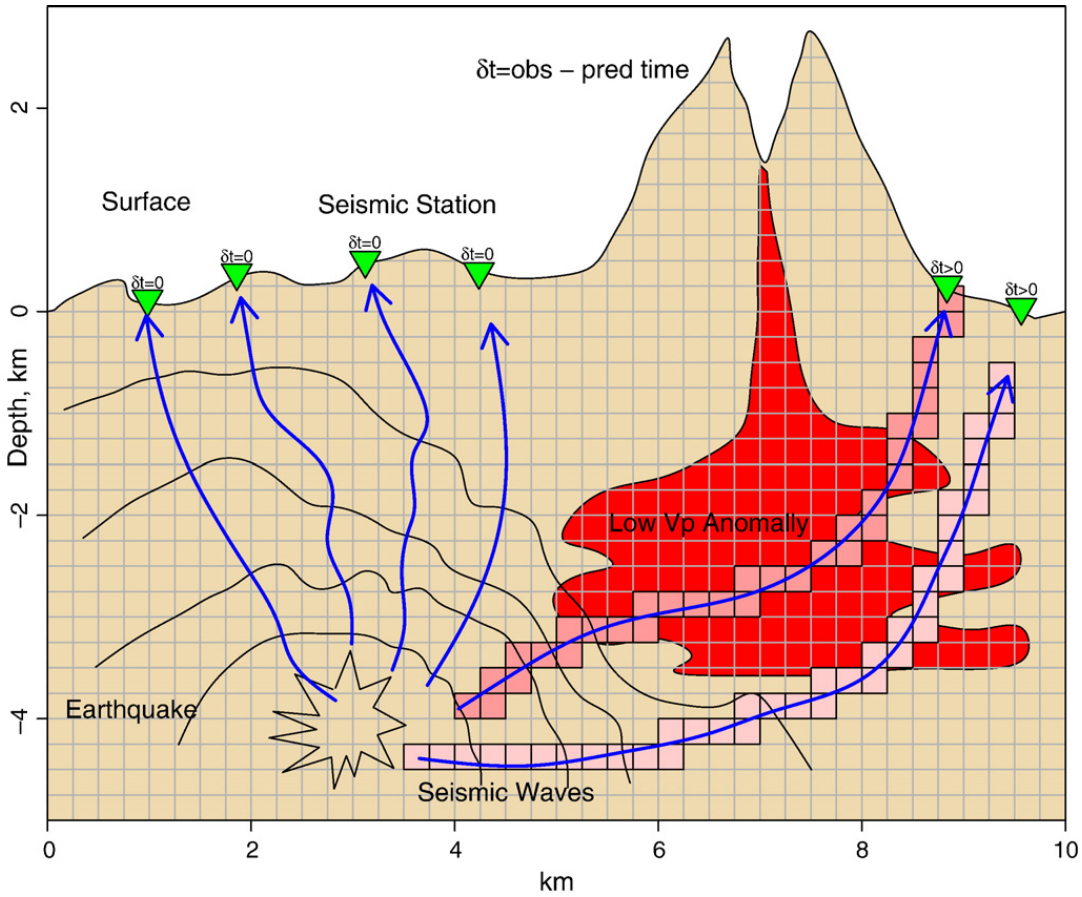

Fig. 1. Cartoon showing earthquake wave-fronts and raypaths used for a tomographic inversion. Raypaths that do not penetrate the anomalous body have a small residual and do not contribute significantly to changing the model. Those ray paths that pass through a low velocity magma region will have a positive anomaly, $\delta t > 0$. The travel-time difference can be projected back along the raypath by distributing the residual along the path. Colored blocks show two different rays intersecting the anomalous region, each with a different level of perturbation. Where paths intersect back-projections will constructively interfere and image reconstruction is attained. (For interpretation of the references to colour in this figure legend, the reader is referred to the web version of this article.)

the observed quantity under study, called the residual, is distributed along the length of the ray in the body of the target region. As seismic waves traverse across subsurface structure, positive and negative anomalies are constructed where the residuals share the same sign and agree and are diminished or canceled where the residuals diverge. An image is built up by numerous crossing rays adding constructively. It can be shown that if one has perfect coverage, the image of the target region can be completely recovered (Deans,1983). Of course, in reality ray coverage in all tomographic analyses is well below perfection and resultant images are blurred and smeared. Blurring and image degradation is naturally much worse in the earth sciences than in medical fields.

Seismic tomography comes in two main forms, although there are some exceptions. The most straightforward inversions involve finding seismic velocity from travel-time anomalies. These include both P- and S-wave arrival times and in some cases joint inversions of both these structures are accomplished by considering V_p/V_s ratios. In some cases it is possible to estimate the attenuation waves have experienced along the travel path and then seismologists attempt to delineate the amplitude attenuation of the intervening material. Usually we seek the inverse of attenuation, Q (quality factor) that measures the relative amount of energy passing through material over one wavelength or period. Q inversion is not inherently non-linear and hence more closely resembles medical imaging. In a few rare cases researchers have succeeded in finding structures related to the anisotropic structures in the subsurface, usually associated with fracture density (Lees and Wu, 1999). While travel-time tomography is inherently non-linear and requires iterative convergence to a final solution, Q tomography is simpler. Estimating attenuation, however, on seismic signals is much more difficult than estimating arrival times and so Q analysis is less commonly applied.

The hope in a volcano tomographic inversion is that we will be able to delineate structure, i.e. the shape and geometry of magma accumulations. This is usually accomplished by deriving a three dimensional image, i.e. a grid of points with value assigned to each one representing a physical parameter. In some schemes nodes (or functions) are derived and parameters are represented by combinations of nodes. The three-dimensional (3D) grid is often called a 'model' because it represents an idealized, digitized version of the real earth, derived via some complex set of calculations or inversion. Structure is then determined by contouring the 3D model and delineating regions with similar properties, such as high and low velocity anomalies. Numerical values, or amplitudes, of anomalous 3D variations may then be interpreted in terms of physical parameters (fluid saturation, lithology, melt percentage, etc.). The second, interpretive step usually relies on external, *a priori* information, sometimes obtained empirically via laboratory observations or through theoretical considerations.

Arrival times of seismic waves from earthquakes are the simplest and most precise measurements made on seismic records. Earthquake locations depend on the ability to determine travel times of events, which in turn require knowledge of seismic velocity structure in the intervening media. Generally, earthquakes are initially located with one-dimensional, layered models since the earth is strongly stratified. While these event locations are reasonably good for general purposes, the earth, of course, is three-dimensional and 3D tomography is an attempt to take this into account. To improve our understanding of structural details in the field we seek a 3D model that explains the data (travel times) better than the one-dimensional model, and provides information on the three-dimensional variation of seismic properties in the earth.

In seismology the relationship between the travel time and the velocity of the medium can be written simply as,

$$\Delta T = \int_{\text{ray}} \frac{1}{V(\text{ray})}\,\text{dl} = \int_{\text{ray}} S(\text{ray})\,\text{dl} \qquad (1)$$

where ΔT is the travel time, V is the velocity (S is the inverse velocity or slowness), dl is an element along the raypath and the path integral is taken along a line perpendicular to the wave-front, called the ray. We often introduce the slowness (S), the reciprocal of the velocity, to avoid the $1/v$ relationship. The 'inversion' is an attempt to extract the velocity given the travel-time data. In Eq. (1) the dependence of the velocity on the raypath is made explicit to emphasize that seismic travel-time tomography is inherently non-linear because the paths of the rays from earthquake source to the receivers depend on the model parameters (velocity) that are being sought. Traditional medical CAT-scanning, furthermore, is accomplished by inverting slices of the target region and building three dimensional models by stacking series of 2D models (the word tomography means 'slice picture'). In seismology, 3D structures are typically determined via full 3D inversion, and later they are sliced for visualization purposes.

Tomographic analysis for velocity anomalies begins by locating earthquakes (sources), usually with one-dimensional models. Raypaths from sources to receivers are calculated and the target region is divided, or parameterized, into small cells. For each raypath a weighting function is determined which estimates the influence of

the data for that ray on the cells in the model that the ray traverses. For block models, this amounts to estimating the penetration length of each cell the ray intersects. The travel-time residuals, i.e. the difference between the predicted travel time and the observed travel time (Fig. 1), are then projected along the raypath along the cells according to the weighting function. In the computer this can be expressed as a large, sparse matrix inversion. Because the raypaths and earthquake locations depend on the velocity models, the inversion is non-linear and a solution is achieved by iteration of linearized steps which converge to the final solution. The size of the matrices can often be quite large (50,000 model parameters) and model resolution and error bars are usually estimated via computational approximations and simulations.

While simple travel times provide the basis for velocity analysis, the amplitudes and frequency content (spectrum) of seismic waves contain rich information on the absorption of seismic energy in the intervening media. Seismic velocity tends to be a relatively insensitive estimator of temperature variations in rocks. Attenuation, on the other hand, is a relatively sensitive indicator of rock temperature (Evans and Zucca, 1993; Sanders et al., 1994). Usually physicists measure the 'quality factor' of materials, i.e., the efficiency of the material to pass energy at a particular frequency. The quality factor, Q, is defined as the ratio of stored to dissipated energy in material as seismic waves propagate through. Attenuation is then defined as the reciprocal of Q and thus represents a measure of the absorption or loss of energy in the seismic waves as they pass through intervening material. Q values range typically from 10 to 100 in laboratory measurements on sandstones and 100–1000 in igneous and metamorphic rocks (Johnston et al., 1979). These measurements, naturally, are performed on simple samples and do not take into account large scale structures, fractures and mixtures.

Attenuation usually comes in two guises: intrinsic and scattering. Intrinsic attenuation relates to losses associated with heat and friction. Scattering attenuation is due to losses from waves diffracted throughout the medium as they propagate from source to receiver. This implies that we may interpret 3D Q variations as being related to intrinsic physical properties of the rocks such as lithology, temperature, and porosity.

2. Inversion approach

Nearly all seismic tomography is founded on a linearization of the highly non-linear seismic inversion problem. In Eq. (1) it was noted that the raypath depended on the velocity model which also depends on the raypaths in the inversion. Furthermore, earthquake locations are also derived using the velocity models, so this introduces an additional non-linearity. To circumvent the nonlinearity we usually introduce a linearization of the inversion and iterate a sequence of linear inversion in the hopes that we will converge to the correct non-linear solution. This is accomplished by assuming we have a reasonably close initial guess to the correct solution and then seeking a small perturbation which will drive the model closer to the correct, final model. The sequence of calculations involves making an initial (typically 1D) model, finding the raypaths in that model, perturbing the (3D) model so the travel times are minimized, adding new perturbations to the first model and iterating. Once the new model is derived, new earthquake locations are calculated and the process is repeated. These iterations usually converge in a few to several steps. Convergence is determined when the models change by a very small amount between iterations and travel-time differentials get small.

The inversion described above is typically discretized (digitized) by assuming the earth is composed of blocks, or nodes of points, where the velocity is defined. The integrals in Eq. (1) can be discretized and cast in matrix form. The matrices involved include a data design matrix which describes the way the raypaths intersect the earth model and the data (travel-time perturbations), i.e. the differences between the observed travel times and calculated times through the current model. New, upgraded, models are derived by least-squares methods. Since the matrices are very sparse, specialized methods have been developed to store the data and arrive at an inverse solution with great speed.

3. Methodology and inversion

Once all the data are collected and the relationship of the intersecting ray paths with the target region is discretized and digitized, a set of matrices is typically set up to solve the so called inverse problem: what earth model would give rise to the travel-time residuals observed. If we represent the earth model as a vector of perturbations (anomalies), $\mathbf{x}$, the interaction of the raypaths with the earth as $\mathbf{A}$, the array of travel-time residuals, $\Delta\mathbf{t}$, one can relate the earth to the residuals by the simple linear relationship,

$$\Delta\mathbf{t} = \mathbf{A}\mathbf{x}. \tag{2}$$

This matrix equation is solved using a variety of methods depending on the structure of the matrices, although the specific approach usually does not have a

large impact on the resulting images. In this review I am concentrating on magma chambers and tomography and the mathematical and computational details are less important for this purpose. A few important comments are in order, however, to understand some of the limitations of tomographic methods.

4. Error

There are two important aspects of every inversion problem that must be addressed before one can interpret a tomographic image. The first has to do with estimation of the errors of the perturbations derived. The second has to do with the resolution, or smearing, of the final result, as compared to an ideal image if perfect coverage were available. Every three-dimensional analysis must account for error and resolution to be complete. Unfortunately, most tomographic inversions involve matrices that are so large that formal calculation of error and resolution are not feasible and often approximate methods are used.

There is noise in all geophysical measurements. Even though the onset of P-wave seismic arrivals is one of the most precise observations made in earth science, it is still plagued by the presence of noise and uncertainty. This may arise because of human error or may be a result of limitations in frequency bandwidth of the recorded waves. Waves arriving from nearly the same source (earthquake) at the same station may not produce exactly the same travel-time observations. This leads to inconsistency in the large matrix inversion. Inconsistency in the design matrix will create large, undesired fluctuations in the resulting images. To avoid this, researchers typically damp or filter during the inversion process. Simple damping (damped least squares) is often applied by constraining the inversion to keep perturbations small. More sophisticated methods using filtering constrain models to conform to some preconceived or *a priori* notion of what one would expect in the images. The generic term encompassing all mathematical methods for controlling the effects of errors is called "regularization". Regularization is usually implemented by smoothing or requiring images to not have large gradients. The implication of this approach to regularization is that the tomographic images usually have smooth boundaries — sharp edges are excluded *a priori* via the imposed condition that large gradients are rejected. In some cases sharp boundaries are known to exist (e.g. the Moho or a fault plane) and this *a priori* information can be incorporated in the inversion by relaxing the regularization along these boundaries. When inversions include damping, values of derived perturbations will be reduced and smoothed out.

In the case of tomographic inversion of magma bodies we generally do not know in advance where sharp boundaries are expected and thus regularization smoothes inversion results significantly. This is important for investigators not familiar with the tomographic methods to understand because it puts limits on the absolute size of observed anomalies. The earth may include perturbations as large as 50% but the regularization constrains observed perturbations to be less than 10%, so the true size of the perturbation is masked by the methodology employed. If the regularizing constraints are relaxed, large fluctuations typically creep in and researchers cannot distinguish between those associated with spurious noise and those related to real anomalies. Tomographic inversion should always be seen as lower bounds on the levels of perturbations in the real earth.

5. Resolution

Resolution is primarily a function of two factors. First is the frequency bandwidth of the incoming seismic signals. Signals that have high frequency sample smaller structures than those of lower frequency. A 5 Hz (1/s) seismic wave traveling in rocks that have seismic velocity of 5 km/s samples objects that have sizes on the order of 1 km. The higher the frequency band the more detail can be extracted. The frequency band of the observed signals is a function of the seismic source, attenuation along the path and bandwidth of recording equipment. Typical earthquake signals in volcanic regions have signals with observed maximum frequency range around 15 Hz.

The second, more important, limitation of seismic tomography is related to ray coverage. Since seismic stations are typically located at the surface of the earth, there is an inherent limitation and constraint on all tomographic analyses on volcanoes. This can be partially compensated for by having earthquakes distributed throughout the target region. Most analyses, however, include earthquake hypocenter distributions that are highly heterogeneous: non-uniform distributions are associated with clustering of earthquakes, often along conduits. The lack of numerous, evenly distributed, crossing rays on the target region causes tomographic images to be biased.

Often earthquakes are clustered and resultant tomographic images depend heavily on this bias. One remedy is to equalize the effect of multiple rays crossing nearly the same path by pre-conditioning the matrix in Eq. (2) by weighting each row according to the number of rays along a certain path (Lees and Crosson, 1989). Bundles of rays are thus grouped together and down weighted

according to the number of rays along a particular path. This has the effect of reducing the influence of closely clustered rays and can improve image quality.

Seismic tomography differs from medical X-ray imaging in one significant aspect: seismic rays bend where velocity gradients are prominent. Since waves preferentially pass through regions of high velocity low velocity regions can be bypassed and thus form a shadow zone. If high accumulations of melt act to lower seismic velocity locally, first arrivals commonly used in travel-time analysis may not sample the very same low velocity regions under investigation. First arrival raypaths bend around low velocity regions. This problem is partially addressed by smoothing and regularization, such that large gradients and sharp boundaries are avoided, *a priori*. Iteration, three-dimensional ray-tracing and final convergence to non-linear models that incorporate low velocities in ray tracing further resolves this problem. Ultimately, the presence of significant low velocities has the effect of further blurring tomographic images.

In summary, resolution and error play an important role at the interpretive stage of tomographic analysis. Formal derivations of both error and resolution are often beyond the computing capacity of many computers and typically underestimate errors in the results (Lees and Crosson, 1991). The introduction of smoothing or regularization will reduce the effects of noisy data at the expense of blurring images and reducing the ability to reconstruct absolute amplitudes of anomalous velocity regions. Non-linear effects further complicate inversions for velocity and earthquake locations, although this is not a problem for attenuation analysis. Attenuation studies, on the other hand, have a higher level of noise than travel-time analysis and are thus not as conclusive.

6. Interpretations and examples

In attempting to relate observed seismic attributes to properties of rocks in volcanic areas several simple rules of thumb are often applied when interpreting tomographic inversions (Sanders, 1993a; Sanders et al., 1995). I should point out that these rules are, by their nature, rather vague because of the complexities and non-uniqueness issues pointed out above. Most laboratory studies are performed in conditions significantly different from real earth situations and at frequencies substantially higher than typical seismic recordings (Mizutani and Kanamori, 1964; Nur and Simmons, 1969; Stocker and Gordon, 1975; Toksoz et al., 1976; Mavko and Nur, 1978; Ito et al., 1979; Winkler and Nur, 1979; Mavko, 1980; Kampfmann and Berckhemer, 1985; Mavko et al., 1998). A comprehensive data base of field based seismic properties related to rock physics laboratory studies is currently not available, so converting seismic field results to three-dimensional variations of rock states is tenuous, at best. In most basic tomographic analyses we expect the presence of increased temperatures to lower velocity for both P- and S-waves. This effect is known to be slight until temperatures approach the melting point and then changes in velocity vary considerably with temperature. For S-waves the velocity may vary by as much as 100% when the sample is completely molten. Fluid saturation generally induces higher P-wave velocity and saturated, unconsolidated sediments typically have high V_p/V_s ratios (Nicholson and Simpson, 1985). Saturation conditions and possibly porosity can thus occasionally be inferred from the comparison of V_p and V_s data (Lees and Wu, 2000). V_p is expected to increase when saturation increases while V_s remains nearly the same, driving V_p/V_s higher (Ito et al., 1979). However, partial melt may decrease V_p and fluid saturated zones will have a net low V_p, low V_s and high V_p/V_s (Walck, 1988). It is evident that competing variations in rock properties and distribution will affect seismic observations in complex ways.

Relating rock properties to observations derived from seismic analysis is particularly difficult because a variety of characteristics give rise to similar variations of seismic features. For the vast majority of tomography studies the seismic parameters under investigation include only four derived properties: velocity and attenuation of P- and S-waves, (V_p, V_s, Q_p, Q_s), and their respective ratios. Ambiguities arise because reducing a myriad of geological and physical processes to four simple seismic observations is non-unique. Laboratory measurements (Sato et al., 1989) and theoretical estimates (Mavko, 1980; Takei, 1998) of seismic wave propagation in the presence of melts show that physical properties vary considerably (Iyer and Dawson, 1993). Lower relative P-wave velocities, for example, may be ascribed to changes in lithology, crystal structure, thermal properties, crack density and the presence of differing phases (Mavko and Nur, 1978; Mavko, 1980; Iyer, 1992; Evans and Zucca, 1993; Iyer and Dawson, 1993). Furthermore, it is well known that perturbations of seismic velocity due to 10% melt vary only by 10–40% for P-waves and can be 20–100% for S-waves (Iyer and Dawson, 1993). The wide range of combinations of properties make it difficult to pinpoint a precise level of partial melt associated with a specific set of parameters. These ambiguities are compounded by computational and analytical difficulties, mentioned above, arising from incomplete coverage and noisy data.

Attenuation (or its reciprocal Q) varies by several orders of magnitude with the presence of melt, but can still

Table 1
Summary of results of tomography on magma systems

Location	Tectonic style	Volcanic products	Type	Result	Analysis type	Citation
Oceanic Ridge						
East Pacific Rise	Oceanic Ridge	Basalt	Ridge	Small, shallow, low V_p	Marine seismic	Toomey et al. (1990)
Juan De Fuca Ridge	Oceanic Ridge	Basalt	Ridge	Low V_p, 6 km^3; 10% melt	Marine seismic	Menke et al. (2002)
Upper Mantle						
Japan	Subduction	Basalt–andesite	Subduction	Numerous low velocity anomalies somewhat correlated to volcanic centers	Subduction seismicity	(Zhao and Hasegawa, 1993; Zhao and Hasegawa, 1993; Iwamori and Zhao, 2000; Zhao et al., 2002)
Kamchatka	Subduction	Basalt–andesite	Subduction	Low velocity somewhat correlated to volcanic centers	Subduction zone eqs	Gorbatov et al. (1999)
Tonga	Back-arc	Basalt–andesite	Subduction	Low V_p	Teleseismic; slab eqs	Zhao et al. (1997)
Cascadia	Subduction	Basalt–andesite	Subduction	Low velocity, low Q_p, correlated to volcanic centers	Regional eqs	Lees and Crosson (1990)
Andes	Subduction	Basalt–andesite	Subduction	Low velocity somewhat correlated to volcanic centers	Teleseismic	Schurr et al. (2003)
Calderas						
Long Valley	Rift	Rhyolite	Caldera	Large small amplitude anomalies associated with the caldera; Low Q_p, Q_s anomalies	Teleseismic and local	(Peppin, 1985; Dawson et al., 1987; Hauksson, 1988; Dawson et al., 1990; Sanders, 1993a,b; Sanders et al., 1994; Steck, 1995; Sanders et al., 1995; Weiland et al., 1995; O'Doherty et al., 1997)
Yellowstone	Hot Spot	Rhyolite–basalt	Caldera	Low V_p, V_s 1–3% anomaly; low Q_p	Teleseismic	(Iyer et al., 1981; Benz and Smith, 1984; Clawson et al., 1989; Miller and Smith, 1999; Husen and Smith, 2004; Yuan and Dueker, 2005)
Valles	Rift	Rhyolite	Caldera	Shallow low velocity; deep low V_p 12–15 km depth	Teleseismic	Lutter et al. (1995)
Taupo	Subduction	Dacite	Caldera	No clear low velocity anomaly		Sherburn et al. (2003)
Rabaul	Subduction	Basalt–andesite–dacite	Pyroclastic shield	Low V_p 3–6 km depth	Local	Finlayson et al. (2003)
Toba	Subduction	Basalt–dacite	Caldera	Low velocity 37%	Local	Masturyono et al. (2001)
Iceland						
Krafla	Rift	Basalt	Caldera	Shallow low velocity	Local	(Einarsson, 1978; Foulger and Arnott, 1993)
Hekla	Rift	Basalt	Stratovolcano	No significant anomalies	Local	Soosalu and Einarsson (2004)
Torfajökull	Rift	Basalt	Stratovolcano	No significant anomalies	Local	Soosalu and Einarsson (2004)
Hengill–Grensdalur	Rift	Basalt	Crater rows	10% low velocity	Local	Toomey and Foulger (1989)
Cascadia						
Newberry volcano	Subduction	Basalt–rhyolite	Shield volcano	Low V_p<10%	Local; synthetic	(Achauer et al., 1988; Stauber et al., 1988)
Medicine Lake	Subduction	Basalt–rhyolite	Shield volcano	Low V_p<10%	Local; active source	(Evans and Zucca, 1988; Lees and Crosson, 1989; Ritter and Evans, 1997)

(continued on next page)

Table 1 (*continued*)

Location	Tectonic style	Volcanic products	Type	Result	Analysis type	Citation
Cascadia						
Mt. St. Helens	Subduction	Andesite–dacite and occasional rhyolite	Stratovolcano	High V_p 20% top of stopoing zone; Low V_p conduit and deep Low V_p	Local earthquake	Lees (1992)
Mt. Rainier	Subduction	Granodiorite–andesite	Stratovolcano	Low V_p 8–15 km	Local–regional eqs	(Lees and Crosson, 1990; Moran et al., 1999)
Alaska						
Redoubt	Subduction	Basalt–dacite	Stratovolcano	10% perturbations; no clear magma body	Local eqs	Benz et al. (1996)
Japan						
Unzen	Rift	Basaltic	Complex volcano	Low V_p	Local–regional eqs	Ohmi and Lees (1995)
Onikobe	Subduction	Basalt–dacite	Volcanic chain	Low V_p, V_s, high V_p/V_s	Local eqs	Nakajima and Hasegawa (2003)
Kirishima	Subduction	Basalt–dacite	Shield volcano	High and low velocity; low Q	Local–regional eqs	Yamamoto and Ida (1994)
Nikko-Shirane	Subduction	Basalt–dacite	Shield volcano	30% low V_p 5–15 km depth	Local eqs	Horiuchi et al. (1997)
Mt. Fuji	Subduction	Basalt–dacite	Stratovolcano	Low V_p below summit	Local–regional eqs	Nakamichi (2005)
Kamchatka						
Klyuchevskoy	Subduction	Basalt–dacite	Stratovolcano	Low V_p 25–40 km depth	Local–regional eqs	(Anosov et al., 1978; Ozerov, 2000)
Hawaii						
Halemaumau	Hot Spot	Basalt	Shield	Low V_p 6 km deep	Local eqs	Rowan and Clayton (1993)
Kilauea	Hot Spot	Basalt	Shield volcano	Low V_p, High V_p in shallow conduit	Local eqs	(Thurber, 1984; Rowan and Clayton, 1993; Okubo et al., 1997; Haslinger et al., 2001)
Italy						
Vesuvius	Subduction	Basal–dacite	Somma volcano	No shallow anomaly; Low V_p at 8 km depth	Local eqs	(De Natale et al., 1998; Zollo et al., 1998)
Campi Flegrei	Subduction	Basalt–dacite	Caldera	Low velocity 3–4 km; gas accumulation?	Local eqs	1988; Aster et al., 1992
Mt. Etna	Subduction	Basalt–dacite	Stratovolcanoes	High velocity	Local eqs	(Cardaci et al., 1993; Villasenor et al., 1998; Laigle and Hirn, 1999; Chiarabba et al., 2000; Aloisi et al., 2002)
Indonesia						
Pinatubo	Subduction	Basalt–dacite	Stratovolcano	Low V_p 6–11 km depth; 15% anomaly	Local eqs	Mori et al. (1996)
S. America						
Nevado del Ruiz	Subduction	Basalt–dacite	Stratovolcano	Low V_p and V_s	Local eqs	Londoño and Sudo (2003)
Tungurahua	Subduction	Andesitic	Stratovolcano	High V_p in upper 4–5 km	Local eqs	Molina et al. (2005)
Canary Islands						
Gran Canaria	Hot spot	Basaltic	Fissure vents	No low velocity	Local eqs	Krastel and Schmincke (2002)

be elusive for interpretation as a variety of physical processes can give rise to amplitude decay. We are usually most interested in intrinsic attenuation, i.e. attenuation associated with absorption due to frictional heat loss, but scattering can play a significant role in the real earth and is often not taken into account in laboratory analyses. In some cases intrinsic attenuation has been shown to be prevalent (Wu and Lees, 1996), but this is certainly not always the case. The presence of gasses such as H_2O and CO_2, occasionally invoked to explain seismic anomalies, further complicates matters. Attenuation of water saturated rocks has been measured extensively in laboratory conditions and used in tomographic studies of fault zones to isolate asperities (Lees and Lindley, 1994), but these effects are not likely to be applicable to investigation of the deeper crust where magma bodies reside.

Thus, the inherent non-uniqueness of tomographic interpretations requires some form of *a priori* information to constrain possible interpretation options. In volcanic regions the approach has been to ascribe low velocity, high attenuation (low Q) to magma accumulation and high velocity, high Q, to either, cooled magma dykes, conduits, plugs or extinct chambers, or to other lithologic variation. Occasionally surface geological observations are used to constrain interpretations, although this is less useful because the targets for tomographic inversion are generally too deep to have surface exposure. More often, surface correlation to geologic structure is used to justify an interpretation of more speculative features far from ground truth.

7. Applications

Extensive reviews and examples of application of tomographic methods have been collected in compilations and review articles (Iyer and Hirahara, 1993). In particular, earlier discussions of tomographic inversion are reviewed in several papers from that compilation (Evans and Zucca, 1993; Foulger and Arnott, 1993; Iyer and Dawson, 1993; Sanders, 1993a; Thurber, 1993). As data collection is constantly improving and computed tomography grows and expands, I cite and review here several cases published since 1993, although my list is surely not exhaustive (Table. 1). In summarizing I have tried to highlight the main features as they pertain to the delineation of melt accumulate, conduits, dykes and/or sills.

8. Mid-ocean ridge inversion

Tomographic inversion of magma accumulations at Mid-ocean ridges are usually conducted using active source tomography. In these cases stations are located at the ocean bottom or recorded as pressure fluctuations using hydro-phones. Examples include images of the East Pacific Rise (Toomey et al., 1990) where only a very narrow low velocity body was found around 3 km depth. In nearly all these cases a shallow, low velocity zone was identified, although a large broad body of rising thermal anomaly is usually absent. Imaging of the Juan De Fuca Ridge (Menke et al., 2002) suggests there is a minimum magma chamber of volume ~ 6 km^3 estimated at 10% melt and, including a more northerly coaxial extension, a total melt volume as large as ~ 1 km^3 for the region imaged. In both these cases the total volume of magma chambers and melt volume are relatively small considering the massive amounts of magma reaching the surface.

9. Upper mantle subduction zone anomalies

Subduction zones offer an attractive target for seismological examination of magma generation and the early formation of magma bodies. Several regions have been investigated for three-dimensional structures related to magma accumulation in the upper mantle and deep crust above subduction zones, including Japan (Zhao and Hasegawa, 1993; Zhao et al., 1994; Iwamori and Zhao, 2000; Zhao et al., 2002), Kamchatka (Gorbatov et al., 1999), Tonga (Zhao et al., 1997), and the Puget Sound (Lees and Crosson, 1990). There seems to be a general correlation of seismic low velocity anomalies and volcanic centers in these images, although the relationship is not strict. Since images are generally amorphous and resolution in the upper mantle is relatively low compared to the distribution of individual volcanic centers at the surface, correlating volcanic centers with upper mantle seismic anomalies is a matter of broad interpretation. Attenuation of P-waves in the Andean subduction zone (Schurr et al., 2003) shows complex ascent paths, not simply vertical conduits to the surface volcanoes. The authors interpret anomalous 3D variations of Q_p as fluid and melt accumulations in the mantle wedge of the subduction zone. Anomalous structures in the wedge again appear to be large blobs extending tens to about 100 km in vertical and lateral extent. These examples offer little in the way of delineating the extent and amount of partial melt in potential magma chambers.

10. Focused inversions

Caldera systems that have erupted large quantities of material have been the target of numerous studies of seismic velocity and attenuation inversion. These include, for example, Long Valley (Peppin, 1985; Dawson et al., 1987; Hauksson, 1988; Dawson et al., 1990; Sanders,

1993b; Sanders et al., 1994; Sanders et al., 1995; Steck, 1995; Weiland et al., 1995; O'Doherty et al., 1997), Yellowstone (Iyer et al., 1981; Benz and Smith, 1984; Clawson et al., 1989; Miller and Smith, 1999; Husen and Smith, 2004; Yuan and Dueker, 2005). In both these cases low velocity and high attenuation was observed in the expected regions, although the magnitude of anomaly has always proven to be lower than anticipated from projections of magma accumulation based on eruption products. Furthermore, details of the storage system have been poorly resolved because of ray and station coverage issues as described above. At Valles caldera, shallow low velocity anomalies and a larger, 12–15 km anomaly at the base of the crust were identified and interpreted as possible magma accumulation or heat perturbations (Lutter et al., 1995).

At active volcanoes, where seismicity is relatively high and local seismic arrays are dense enough, we have the best potential of observing details of magma plumbing systems. Numerous volcanoes and volcanic regions have been investigated in this manner and here we cite several notable localities where at least some form of low velocity was observed and interpreted as evidence for magma accumulation.

11. Large calderas

Seismic tomography at Taupo Caldera, the largest active rhyolitic complex in the world, failed to show significant presence of melt accumulates. No clear low velocity anomalies associated with magma or melt in the upper levels of the Taupo Volcanic zone were identified by Sherburn et al. (2003). The authors suggest that the presence of higher velocities indicate older intrusives and prominent low velocities are related to caldera collapse structures and possibly geothermal variations (Wu and Lees, 1999).

On the other hand, a significant 30–35 km^3 volume of low velocity anomaly at 3–6 km below Rabaul Volcano was interpreted as evidence for appreciable accumulation of melt (Finlayson et al., 2003). Higher velocities on the rim of the caldera were again interpreted as intrusive mafic rock. The authors further noted that a lack of low velocity anomalies below Tuvai caldera (15–20 km north of Rabaul) suggested this was inactive and thus posed no threat of eruption.

At the Toba caldera complex in north Sumatra, tomographic studies using a local array show crustal low velocity anomalies up to 37% that coincide with gravity anomalies in the region (Masturyono et al., 2001). Low velocity anomalies were observed to be separated by a high velocity structure and the authors suggest that perhaps two magma accumulations are being imaged. The apparent shallow magma bodies are interpreted as representing regions of partial melt that may be connected to low velocity anomalies observed in the upper mantle below Toba, indicating a connection from the mantle to the crust, possibly a feeding system. This rare observation is exceptional and suggests that further investigation at other large caldera systems should be pursued.

12. Iceland

In Iceland several tomographic inversions have been applied to investigate the large scale structure, as well as smaller scale features associated with specific volcanic centers. Early teleseismic studies of the Iceland plume showed significant anomalies in the upper mantle associated with a tube-like mantle plume (Tryggvason et al., 1983). Later large scale tomographic imaging (Foulger et al., 2001), aimed at illuminating the mantle plume, showed that mantle structure below the hot spot does not include a simple, tube like conduit from the core–mantle boundary to the surface, but rather a complex and broadened blur of low velocity extending to 600 km depth is seen. Menke et al. (1995) used attenuation and also found no evidence of a large attenuating body below Iceland as might be expected for a region of major volcanic activity.

Tomographic inversion at Krafla Volcano indicates shallow low velocity conduits with significant velocity perturbations that lie above a possible 3–7 km deep magma chamber indicated by S-wave attenuation (Einarsson, 1978). Toomey and Foulger (1989) looked at local earthquake waveforms to image the velocity structure at Hengill–Grensdalur region east of Reykjavik. They found several high velocity bodies and a smaller 3–4 km wide low velocity body (−10 to −7%) below Hengill interpreted as a region of partial melt.

At Hekla and Torfajökull seismic surveys showed no evidence of large magma accumulations in the range of 5–14 km depth (Soosalu and Einarsson, 2004). The authors excluded the possibility of there being large volumes of molten material under either of these eruptive centers unless the magma chambers are either very deep (>14 km), or, in the case of Hekla, quite shallow. These puzzling conclusions inspired the authors to suggest other targets near the volcanoes as potential sources for the plumbing system of the calderas.

13. Hawaii

Using teleseismic inversion in Hawaii, Ellsworth and Koyangi (1977) conducted one of the earliest tomographic analyses on a volcanic region. A laterally extensive

conduit system serves as a plumbing complex where low velocity anomalies were observed below volcano summits at 27–43 km depth. Large accumulations of magma at Kilauea were not interpreted in the 12–25 km range. Other velocity analyses have each observed various low velocity bodies below Hawaiian volcanoes although none has convincingly identified a deep low velocity on this active hot spot (Thurber, 1984; Rowan and Clayton, 1993; Okubo et al., 1997; Haslinger et al., 2001). Haslinger et al. (2001) found a deep low velocity body around 9 km depth that they offered as a possible locus of melts — estimating a 10% melt accumulate or a 500° perturbation of temperature. Rowan and Clayton (1993) observed a 6 km deep shallow plexus of tubes 2 km southeast of Halemaumau caldera surrounded by higher velocity features. More recently, much more detailed analyses using local events along the East Rift Zone have showed low V_p, low V_p/V_s, high Q_p and low Q_s, although the authors suggest that this anomaly is related to CO_2 accumulation rather than the presence of magma.

14. Italy

Several studies of the subsurface of Vesuvius include detailed 2D and 3D tomographic analysis (De Natale et al., 1998; Zollo et al., 1998). These analyses, however, did not show significant P- or S-wave low velocity anomalies in contrast to earlier estimates based on the substantial amount of melt that should be present following plinian eruptions. The authors suggested that an anomalous region at 8 km depth, extending from 10 to 25 km laterally around the summit, represents a deep magma accumulation region which plays a role in feeding the volcanic plumbing system. In a more detailed analysis of earthquake and artificial sources De Natale et al. (2004) found high V_p/V_s ratio with high V_p related to regions of higher seismicity. They interpreted this as a region of quenched magma, perhaps still at relatively high velocity. No evidence of a deep magma body in the range of 10–15 km was evident from their modeling. Potential field methods (Iuliano et al., 2002) further showed a narrow conduit in the top 5 km of Vesuvius, although no strong evidence of a deep seated large magma system was observed. In summary, the Vesuvius region shows little or no sign of a low velocity/high attenuation shallow magma body. A deeper region is suggested although not well imaged, and speculation still remains as to the connection of the deeper magma storage area and the shallow high velocity region.

The Campi Flegrei area was imaged originally by Aster and Meyer (1988) (Aster et al., 1992), who found low P-wave and S-wave velocity layers at 3–4 km depth. They suggest that the 4 km maximum depth of seismicity indicates that if a large magma body exists below Campi Flegrei it must be below this depth. Later Vanorio et al. (2005) found no evidence of large magma bodies and interpreted low V_p/V_s as gas accumulation. Furthermore, no evidence of any considerable chamber of magma was observed by Zollo et al. (2003) in a study of active source tomography at Campi Flegrei caldera. Attenuation studies also did not find any evidence of a large magma accumulation or high percent melt at Campi Flegrei (de Lorenzo et al., 2001). In a teleseismic study over the whole Campanian volcanic region, a small low velocity anomaly is evident between 15 and 35 km depth below the Vesuvius region (De Gori et al., 2001), although the detailed delineation of this body needs to be examined more closely with localized inversion (other anomalies in this layer on the teleseismic analysis do not specifically relate to obvious magma regions and so may be suspect).

The high velocities at Mt. Etna seem to be consistent over several studies and are almost always interpreted as older intrusives through which new magma systems must penetrate into and mix with prior to reaching the surface (; Cardaci et al., 1993; Villasenor et al., 1998; Laigle and Hirn, 1999; Chiarabba et al., 2000; Aloisi et al., 2002). The presence of high velocity anomalies is not uncommon in several tomographic inversions and can be puzzling for large volcanoes such as Etna.

15. Cascades

Cascade volcanoes have been the target of numerous studies to estimate the three-dimensional extent of magma bodies feeding the active volcanoes. Notable in the southern Cascades are Newberry volcano (Achauer et al., 1988; Stauber et al., 1988) and Medicine Lake (Evans and Zucca, 1988; Ritter and Evans, 1997). These works involved inversion of active source (man made explosions) seismic records and local earthquakes. In both cases low velocity anomalies were observed in the vicinity of the central regions of the volcano edifice, although these in general appear to be typically less than 10% in value.

In Washington State tomographic inversion of the Puget Sound region showed anomalously low velocity at Mt. St. Helens and Mt. Rainier. In more detailed studies of Mt. St. Helens, Lees found low velocity anomalies deep in the crust and heterogeneous perturbations distributed beneath the volcano edifice. In perhaps one the of the most detailed tomographic inversions of a volcanic area Lees and Crosson (1989) and Lees (1992) found a high velocity anomaly at the top of the magma chamber outlined using earthquakes (Pallister et al., 1992) and a low velocity beneath, starting at 9 km depth (Fig. 2). It was speculated

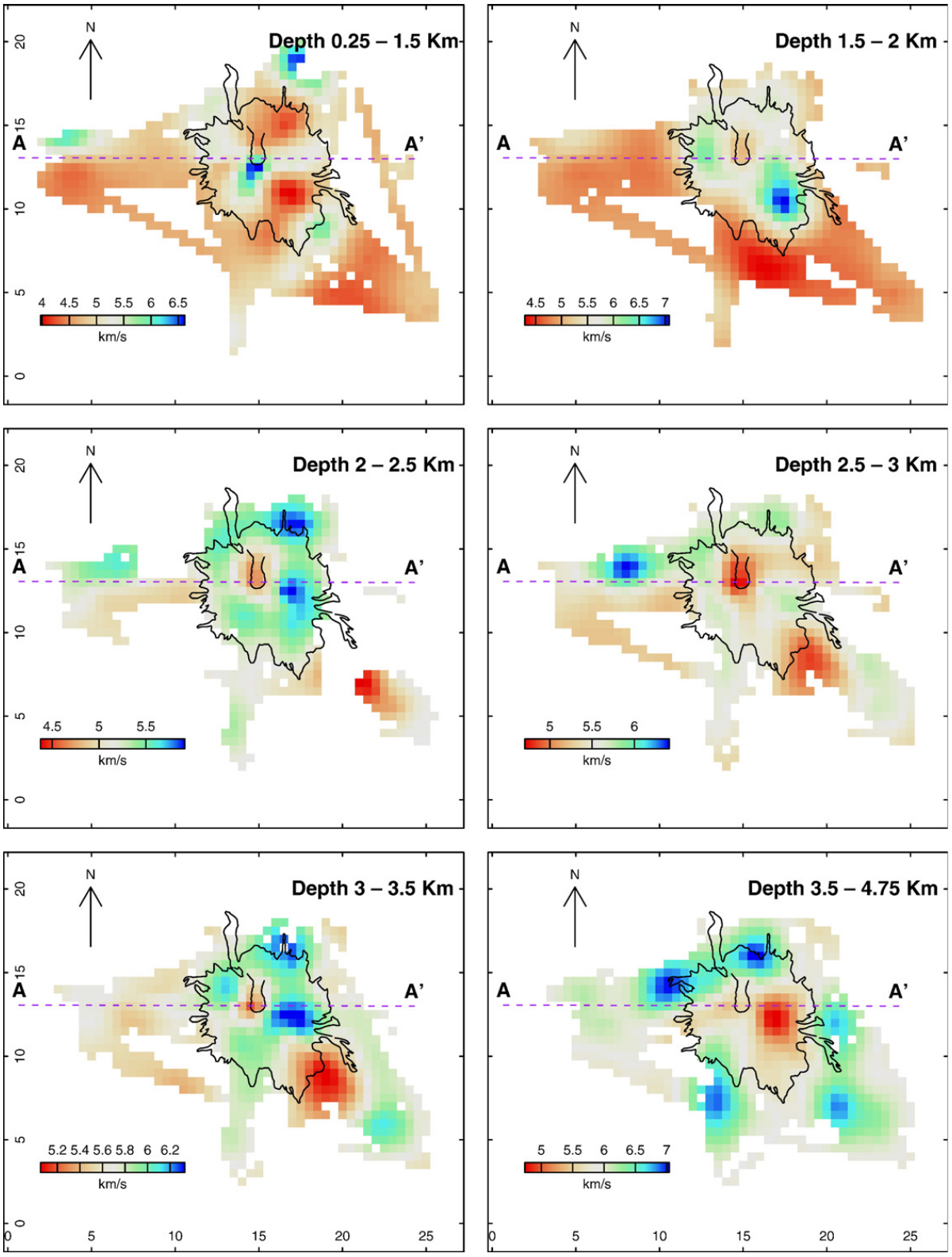

Fig. 2. Tomographic inversion at Mt. St. Helens (Lees, 1992). Velocity is represented by colored blocks scaled according velocity distribution in layers. Part A represents a series of horizontal slices through the model at layers defined by the one-dimensional background model. Part B is a vertical cross section through the model trending west to east. Lines drawn on the vertical section were digitized from Pallister et al. (1992) and superimposed for comparison. In the vertical cross sections the difference between absolute velocity and perturbation anomalies is illustrated. (For interpretation of the references to colour in this figure legend, the reader is referred to the web version of this article.)

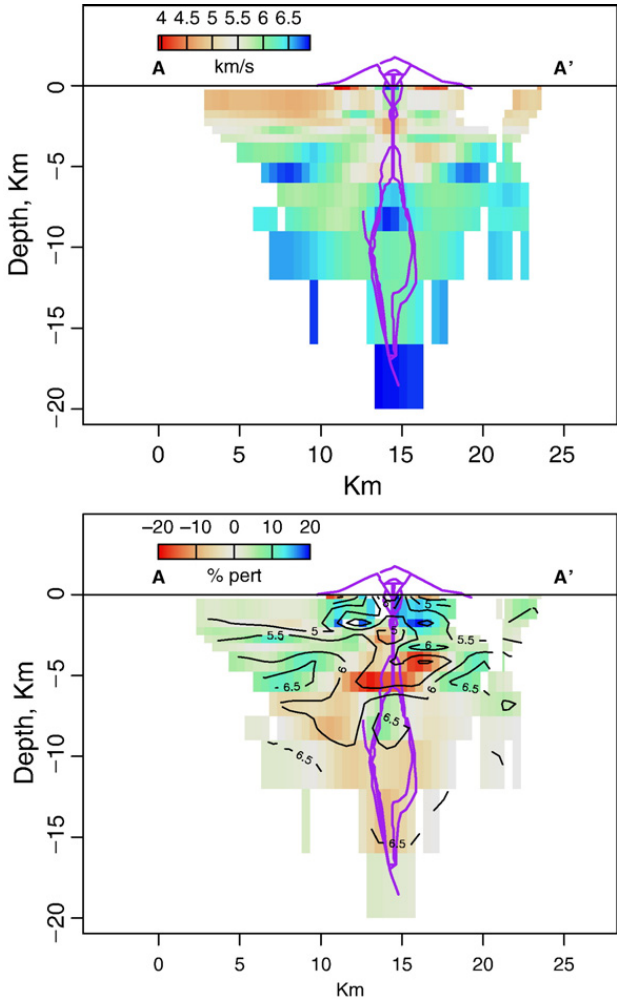

Fig. 2 (*continued*).

that the high velocity anomaly represents an extinct magma body through which new dykes penetrated during the 1980 eruption. At Mt. St. Helens again anomalies are relatively small in amplitude and clearly do not represent anything remotely resembling a "chamber" of 100% melt. Lees and Crosson (1990) and Moran et al. (1999) both found a significant low velocity anomaly below Mt. Rainier that extends from 8 to 15 km and has a lateral extent at least 15 km in the east–west orientation and more in the north–south direction.

16. Redoubt

A detailed study of travel-time tomography at Redoubt volcano exhibited perturbations on the order of ±10% although a clearly defined magma body was not evident (Benz et al., 1996). Rather, pipe-like structures in the shallow regions and a low velocity "magma plexus" was reported and offered as support for a system of dykes and conduits for magma feeders. The authors noted correlations between velocity anomalies and volcanic tremor, especially low frequency events.

17. Japan

Ohmi and Lees (1995) used local earthquake data to invert for velocity anomalies prior to the disastrous pyroclastic flows of 1991 at Unzen Volcano in the Shimabara Peninsula off Kyushu, Japan. They found a significant low V_p anomaly below Unzen crater extending from the surface to 15 km depth. The low V_p anomaly is most prominent slightly southeast of Unzen summit and the authors postulated that a system of conduits and dykes comprise the shallower low velocity perturbations. Below Unzen the dense Chijiwa bay earthquake swarm occurs in a high velocity zone northwest of the volcano, assumed to be outside of the magma accumulation and responding to tectonic stress in solidified rock.

Tomographic studies of Onikobe Volcano, northeastern Japan, showed low velocity anomalies in narrow conduits below Naruko volcano and deeper low velocity anomalies, although the authors argued that low V_p/V_s ratio observed there indicated the presence of heated H_2O vapor as opposed to accumulation of melt (Nakajima and Hasegawa, 2003). In the deeper sections of the Onikobe inversion high V_p/V_s ratios suggested the present of melt extending from about 18 km to 45 km. Attenuation at Onikobe (Tsumura et al., 2000) further showed a strong correlation with the low velocity features. At another study around Iwate Volcano, Japan, a fairly shallow (2–4 km below the caldera floor) high velocity anomaly was observed and interpreted as an older, remnant magma system that had cooled and solidified (Tanaka et al., 2002).

Kirishima Volcano, in southern Kyushu, Japan, exhibited a low (15%) velocity anomaly approximately 10 km below the surface interpreted as a magma body (Yamamoto and Ida, 1994). Curiously, a follow up study of the attenuation of seismic waves did not find a corresponding low Q feature (Yamamoto and Ida, 1994). Detailed study of Kirishima volcanic complex (Tomatsu et al., 2001) showed high velocity "pipe-like" structures and high attenuation in the southern part of the target region, although coverage is sparse and anomalies appear as blurred splotches interrupted by unconstrained elements in the model.

A study of the distortion and attenuation of waves passing through the Nikko-Shirane volcano in northern Kanto shows clear evidence for a significant magma region (Horiuchi et al., 1997). In this case perturbations of up to 30% are reported and indicate a large magma body extending from 5 to 15 km with a lateral extent of 5–10 km between Mt. Nikko-Shirane and Mt. Nantai.

Earthquake swarms in this area occur outside the proposed magma chamber to the west above a seismic reflector the authors suggest is a channel for magma flow. While these results are not directly derived from tomographic inversion, the authors point out that tomographic analyses agree with their conclusions (Tsumura, 1995).

For many years monitoring of Mt. Fuji was sparse and seismicity levels were relatively meager. A more regional tomographic inversion by Lees and Ukawa (1992) showed a significant low velocity zone deep (20 km) below Mt. Fuji. In the late 1990's swarms of low frequency earthquakes were recorded in the deep layers below

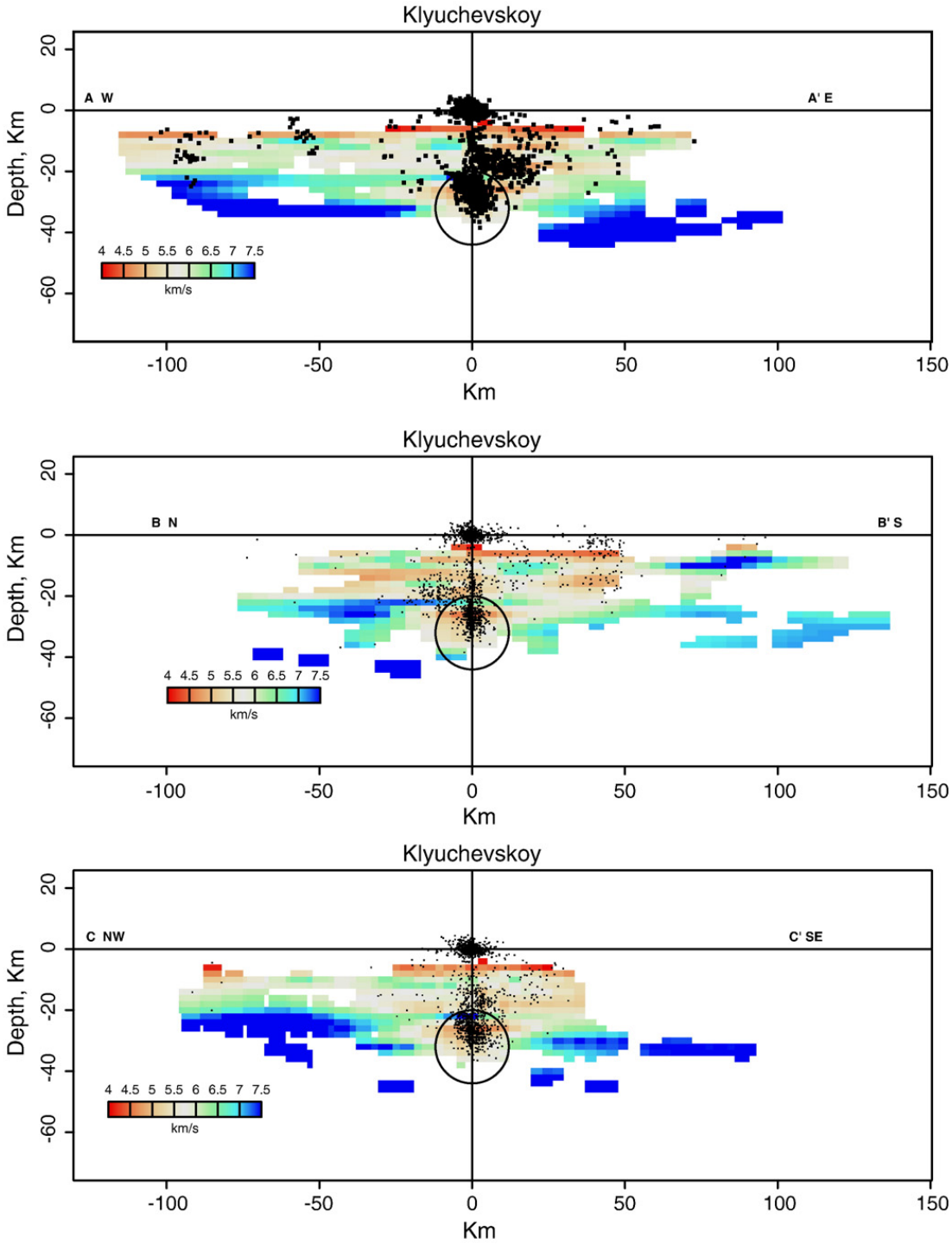

Fig. 3. Tomographic inversion at Klyuchevskoy volcano, Kamchatka, Russia. Three vertical slices through the volcano edifice at different angles are shown for reference. The deep low velocity anomaly (circle) between 25 and 40 km depth may represent a significant accumulation of melt that feeds the large volcanic complex in the central Kamchatka rift valley.

Mt. Fuji (Nakamichi et al., 2004) and seismic networks were improved in the immediate vicinity of the cone. More recent tomographic inversions by Nakamichi (Nakamichi, 2005) exhibit low velocity anomalies below Mt. Fuji's summit, also interpreted as magma accumulation.

18. Kamchatka

Kamchatka represents another understudied volcano target region for detailed seismic studies of magma systems. The great Klyuchevskoy volcano ranks among the largest magma flux regions of the world. Earlier investigations used seismic data to delineate the magma storage at Klyuchevskoy but these did not use 3D analysis known as tomography (Anosov et al., 1978; Ozerov, 2000). More recently Lees et al. (in press) used the local earthquake database to extract images of the magma system and they found significant low velocity anomalies distributed below the Klyuchevskoi–Bezymyany–Tolbachik complex (Fig. 3). Specifically they found a large low velocity concentration immediately below Klyuchevskoy around 25–40 km depth. This was interpreted as a magma chamber, situated at the Moho and feeding the concentrated volcanic center of the Klyuchevskoy group.

19. Pinatubo

Mori et al. (1996) observed low V_p anomalies below Mt. Pinatubo between 6 and 11 km depth that is suggestive of a magma accumulation. Near Mt. Negron they postulate a smaller (15–25 km^3) reservoir over a much larger accumulation (60–125 km^3) below the full Mt. Pinatubo–Mount Negron complex, although the deeper parts of their model are poorly resolved. The images they show range from ±15% and appear to be elongated in the vertical dimension, with a smaller dip component. Hypocenters at Pinatubo appear, for the most part, to be outside of the low velocity features, suggesting that the fluids do not sustain seismic stress which is transferred to the edges. This was also noted at Redoubt (Benz et al., 1996) and Mt. St. Helens (Lees, 1992).

20. South America

Relatively few tomographic studies have been reported for South American volcanic centers and the Andes represent an excellent challenge for our understanding of active magma storage accumulation and transport. The lack of analyses in the Andes may be due to the shortage of infrastructure (seismic networks) and the difficulty of working in such rugged terrain. As seismic stations become less expensive and communication systems easier to deploy we will see increased focus on Andean magma systems. The two studies recounted here concentrate on local structure using earthquakes and small networks. At Nevado del Ruiz, Colombia, shallow high and low V_p and V_s variations were observed below the crater (Londoño and Sudo, 2003). In the 5–10 km zone, however, low V_p and V_s were observed and consequently interpreted as "heat sources". The authors suggest that high V_p/V_s ratios indicate intrusive magma in the range of 3–10 km depth, perhaps representing the magma storage system for this volcano.

Tomography at Tungurahua volcano, Ecuador, illuminated, for the most part, high velocity anomalies in the upper 4–5 km below the summit (Molina et al., 2005). These were construed to be remnant conduit and dyke systems whereas lower velocity material was identified as unconsolidated deposits or fractured volcanic rocks. No evidence was reported regarding an active conduit or magma accumulation. The lack of any evidence for a low velocity conduit or storage area is surprising given the high activity at Tungurahua. I expect that the lack of station coverage is the primary source of this omission, and future studies will see more details, perhaps in the deeper parts of the volcanic complex.

21. Canary islands

At Gran Canaria, Canary Islands, high velocities dominate and are related to intrusives. No clear low velocities were reported and active magma chambers were not considered as part of the analysis (Krastel and Schmincke, 2002). Several anomalous features highlighted here are interpreted geologically as related to alterations during mantle upwelling, although abundant dykes are mentioned below La Isleta peninsula.

22. Summary

In nearly all studies of seismic tomography below active volcanoes or calderas variations of high and low velocity perturbations have been observed and described in varying detail. For the most part, the velocity anomalies can be characterized as amorphous blobs, typical of tomographic inversions in practically all seismic applications. In a few cases relatively detailed conduit geometry has been outlined, but most analyses refrain from interpreting individual, poorly constrained anomalies that are not required by the data. The general rule is to indicate the geographic distribution of broad regions of low and high velocity or attenuation and suggest that higher velocity is associated with older, consolidated volcanic deposits or magmatic intrusion, and lower velocity with partially

molten zone or the presence of other fluids or gasses. Difficulties in interpreting tomographic images where non-uniqueness, multiple models and no ground truth or geological evidence exists represent a severe restriction on using tomography for delineation of magma bodies. Furthermore, inherent problems of incomplete data and non-ideal source–receiver geometry put significant upper bounds on the ability of a seismic data set to constrain subsurface features. The problem of determining of conduit geometry and the presence or absence of magma accumulations has been the major focus of most investigations, although in some cases the much more difficult task of estimating the fraction of partial melt has been attempted. These efforts are fraught with numerous complexities and are, in my estimation, speculative at best.

Most seismic tomography at volcanic regions involves exploring seismic velocity variations and, in some cases, seismic attenuation. While it is not practiced yet, the combination of inverting for all four seismic parameters (V_p, V_s, Q_p and Q_s) simultaneously may offer a possible way to constrain resulting images and improve resolution. This effort is aimed at the continuing effort to include more of the seismic record in the process of connecting earth structure to seismic observations. Ultimately full wave form inversion will be necessary to completely delineate three-dimensional subsurface variations in completely satisfactory manner. In the meantime we are confronted with blurry images and incomplete postulations of the magmatic accumulations that give rise to seismic anomalies.

High velocity anomalies have been observed in shallow crustal regions below numerous active volcanoes (Lees, 1992; Benz et al., 1996; Okubo et al., 1997; Villasenor et al., 1998; Laigle and Hirn, 1999; Chiarabba et al., 2000). These are typically interpreted as either structural features associated with country rock geology or with potentially cooled magma bodies, perhaps remnants of earlier episodes of magmatism below the current summit.

Low velocity anomalies below volcanoes were seen at oceanic spreading centers in the east Pacific (Toomey et al., 1990), Long Valley (Sanders et al., 1995), Yellowstone (Clawson et al., 1989), and volcanoes including Rabaul (Finlayson et al., 2003), Krafla (Foulger and Arnott, 1993), St. Helens (Lees and Crosson, 1989; Lees, 1992), Mt. Rainier (Lees and Crosson, 1990; Moran et al., 1999), Newberry (Achauer et al., 1988; Stauber et al., 1988), Medicine Lake (Evans and Zucca, 1988), Unzen (Ohmi and Lees, 1995), Nikko-Shirane (Horiuchi et al., 1997), Fuji (Lees and Ukawa, 1992; Nakamichi, 2005), Klyuchevskoy (Lees et al., in press), Campi Flegrei (Aster et al., 1992), and Pinatubo (Mori et al., 1996). These were invariably interpreted as evidence for melt accumulation in various forms of dykes, sills or magma chambers. While a few examples showed evidence of shallow low velocity associated with active conduits, most low velocity anomalies attributed to melt accumulates lie deeper in the crust, in the range of 8–15 km depth. The low resolution at these depths often obscure detailed images of the volcanic plumbing systems and more dense seismic arrays are required to image these properly. Overall, there is a general lack of strong evidence for large regions of pure melt below most volcanoes discussed in this review. It is possible that tomographic analyses do not have the resolving power to image melts at high enough resolution with sparse data sets available at this time.

It is also possible that large, consolidated accumulations of 100% melt do not exist in the crust and upper mantle as described in the classic cartoon models used in undergraduate textbooks (Hildreth, 1977; Skinner and Porter, 2004). Cartoon models are simple because they obscure complexities that can confuse an audience unconcerned with details. Furthermore, simplified models offer a way to represent the "magma chamber" as body that can be quantified in geometric terms for physical and dynamic analyses (e.g. (Crosson and Bame, 1985). Either way, the simplifications leave much to be desired and the presence of melt in the crust and upper mantle is likely to be distributed in a complex system of dykes, sills and conduits that may not coalesce into a large clearly defined form (Donnelly-Nolan, 1988). In some cases use of the term "magma chamber" may have to be revised and re-interpreted (Coleman et al., 2004; Glazner et al., 2004). Perhaps a better appellation would be, as geophysicists may prefer, the "blobby zone where the velocity is low and attenuation is high". Alternatively, terms like "magma plexus" (Benz et al., 1996) may supplant older concepts of magma chambers although the name still evokes a sense of vagueness. Furthermore, one definition is unlikely to be applicable to all situations: large caldera systems will have different structures and distributions of magma than smaller explosive volcanic centers.

In this paper I have outlined the difficulties and potential pitfalls in using tomographic methods for defining magma storage systems. While it is still not clear how and where large accumulations of melt coalesce prior to extensive volcanic events, seismological imaging techniques still offer the best hope to determine the geometry and even the percent of melt resident at any given time. The most promising new avenues of investigation will most probably be in using more information from the rich waveform data recorded over magmatic regions in higher density than is available today.

Acknowledgements

Support for this work was provided in part by grants NSF EAR 0337462 and NSF EAR-0440054. The author is grateful for thoughtful reviews by George Zandt, Calvin Miller and an anonymous referee.

References

Achauer, U., Evans, J.R., Stauber, D.A., 1988. High-resolution seismic tomography of compressional wave velocity structure at Newberry Volcano, Oregon Cascade range. J. Geophys. Res. 93 (B9), 10135–10147.

Aloisi, M., Cocina, O., Neri, G., Orecchio, B., Privitera, E., 2002. Seismic tomography of the crust underneath the Etna Volcano, Sicily. Phys. Earth Planet. Inter. 134 (3–4), 139–155.

Anosov, G.I., Bikkenina, S.K., Popov, A.A., 1978. Glubinnoe Seismicheskoe Zondirovanie Kamchatki: Deep Seismic Sounding of Kamchatka (in Russian). Nauka, Moscow. 129 pp.

Aster, R.C., Meyer, R.P., 1988. Three-dimensional velocity structure and hypocenter distribution in the Campi Flegrei caldera, Italy. Tectonophysics 149, 195–218.

Aster, R.C., et al., 1992. Seismic investigation of the Campi Flegrei: a summary and synthesis of results. In: Gasparini, P., Scarpa, R., Aki, K. (Eds.), Volcanic Seismology. Springer-Verlag, Berlin, pp. 462–483.

Benz, H.M., Smith, R.B., 1984. Simultaneous inversion for lateral velocity variations and hypocenters in the Yellowstone region using earthquake and refraction data. JGR. J. Geophys. Res. B 89 (2), 1208–1220.

Benz, H., et al., 1996. Three-dimensional P and S-wave velocity structure of Redoubt Volcano, Alaska. J. Geophys. Res. 101 (4), 8111–8128.

Cardaci, C., Coviello, M., Lombardo, G., Patane, G., Scarpa, R., 1993. Seismic tomography of Etna Volcano. J. Volcanol. Geotherm. Res. 56 (4), 357–368.

Chiarabba, C., Amato, A., Boschi, E., Barberi, F., 2000. Recent seismicity and tomographic modeling of the Mount Etna plumbing system. J. Geophys. Res. 105 (5), 10923–10938.

Clawson, S.R., Smith, R.B., Benz, H.M., 1989. P wave attenuation of the Yellowstone Caldera from three-dimensional inversion of spectral decay using explosion source seismic data. J. Geophys. Res. 94 (6), 7205–7222.

Coleman, D.S., Gray, W., Glazner, A.F., 2004. Rethinking the emplacement and evolution of zoned plutons; geochronologic evidence for incremental assembly of the Tuolumne Intrusive Suite, California. Geology 32 (5), 433–436.

Crosson, R.S., Bame, D.A., 1985. A spherical source model for low frequency volcanic earthquakes. J. Geophys. Res. 90, 10237–10247.

Dawson, P.B., Iyer, H.M., Evans, J.R., Achauer, U., 1987. Inversion of teleseismic travel time residuals to investigate the three-dimensional P-velocity structure of the crust and upper mantle, the Long Valley, California, region. International Union of Geodesy and Geophysics. Gen. Assem. 19 (1), 55.

Dawson, P.B., Evans, J.R., Iyer, H.M., 1990. Teleseismic tomography of the compressional wave velocity structure beneath the long Valley region, California. J. Geophys. Res. 95 (B7), 11021–11050.

De Gori, P., et al. (Ed.), 2001. Teleseismic tomography of the Campanian volcanic area and surrounding Apenninic Belt. J. Volcanol. Geotherm. Res., vol. 109, pp. 55–75.

de Lorenzo, S., Zollo, A., Mongelli, F., 2001. Source parameters and three-dimensional attenuation structure from the inversion of microearthquake pulse width data; Qp imaging and inferences of the thermal state of the Campi Flegrei Caldera (southern Italy). J. Geophys. Res. 106 (B8), 16,265–16,286.

De Natale, G., Capuano, P., Troise, C., Zollo, A., 1998. Seismicity at Somma-Vesuvius and its implications for the 3D tomography of the volcano. In: Spera, F.J., de Vivo, B., Ayuso, R.A., Belkin, H.E. (Eds.), J. Volcanol. Geotherm. Res. , pp. 175–197.

De Natale, G., Troise, C., Trigila, R., Dolfi, D., Chiarabba, C., 2004. Seismicity and 3-D substructure at Somma-Vesuvius Volcano; evidence for magma quenching. Earth Planet. Sci. Lett. 221 (1–4), 181–196.

Deans, S.R., 1983. The Radon Transform and some of its Applications. New York, 289 pp.

Donnelly-Nolan, J.M., 1988. A magmatic model of Medicine Lake Volcano, California. J. Geophys. Res. 93 (5), 4412–4420.

Einarsson, P., 1978. S-wave shadows in the Krafla caldera in NE-Iceland, evidence for a magma chamber in the crust. Bull. Volcanol. 41 (3), 187–195.

Ellsworth, W.L., Koyangi, R.Y., 1977. Three-dimensional crust and mantle structure of Kilauea Volcano, Hawaii. J. Geophys. Res. 82 (33), 5379–5394.

Evans, J.R., Zucca, J.J., 1993. Active source, high-resolution (NeHT) tomography; velocity and Q. In: Iyer, H.M., Hirahara, K. (Eds.), Seismic Tomography: Theory and Practice. Chapman and Hall, London.

Evans, J.R., Zucca, J.J., 1988. Active high-resolution seismic tomography of compressional wave velocity and attenuation structure at Medicine Lake volcano, northern California Cascade Range. J. Geophys. Res. 93, 15016–15036.

Finlayson, D.M., Gudmundsson, O., Itikarai, I., Nishimura, Y., Shimamura, H., 2003. Rabaul Volcano, Papua New Guinea; seismic tomographic imaging of an active caldera. J. Volcanol. Geotherm. Res. 124 (3–4), 153–171.

Foulger, G.R., Arnott, S.K., 1993. Local tomography; volcanoes and the accretionary plate boundary in Iceland. In: Iyer, H.M., Hirahara, K. (Eds.), Seismic Tomography: Theory and Practice. Chapman and Hall, London.

Foulger, G.R., et al., 2001. Seismic tomography shows that upwelling beneath Iceland is confined to the upper mantle. Geophys. J. Int. 146 (2), 504–530.

Glazner, A.F., Bartley, J.M., Coleman, D.S., Gray, W., Taylor, R.Z., 2004. Are plutons assembled over millions of years by amalgamation from small magma chambers. GSA Today 14, 4–11 (April/May).

Gorbatov, A., et al., 1999. Tomographic imaging of P wave velocity structure beneath Kamchatka Peninsula. Geophys. J. Int. 137, 269–279.

Haslinger, F., Thurber, C.H., Mandernach, M., Okubo, P.G., 2001. Tomographic image of P-velocity structure beneath Kilauea's East Rift Zone and South Flank; seismic evidence for a deep magma body. Geophys. Res. Lett. 28 (2), 375–378.

Hauksson, E., 1988. Absence of evidence for a shallow magma chamber beneath Long Valley Caldera, California, in downhole and surface seismograms. J. Geophys. Res. 93 (11), 13,251–13,264.

Herman, G.T., 1980. Image Reconstructions from Projections. Academic Press, New York.

Hildreth, W., 1977. The Magma Chamber of the Bishop Tuff; Gradients in Temperature, Pressure, and Composition. University of California, Berkeley. unknown pp.

Horiuchi, S., Tsumura, N., Hasegawa, A., 1997. Mapping of a magma reservoir beneath Nikko-Shirane volcano in northern Kanto, Japan, from travel time and seismogram shape anomalies. J. Geophys. Res. 102 (B8), 18071–18090.

Husen, S., Smith, R.B., 2004. Probabilistic earthquake resolution in three-dimensional velocity models for the Yellowstone National Park region, Wyoming. Bull. Seismol. Soc. Am. 94 (3), 880–896.

Ito, H., DeVilbiss, J., Nur, A., 1979. Compressional and shear waves in saturated rock during water-steam transition. J. Geophys. Res. 84, 4731–4735.

Iuliano, T., Mauriello, P., Patella, D., 2002. Looking inside Mount Vesuvius by potential fields integrated probability tomographies. In: Spichak, V., Dixon, T., Martin-del Pozzo, A.L. (Eds.), J. Volcanol. Geotherm. Res. , pp. 363–378.

Iwamori, H., Zhao, D., 2000. Melting and seismic structure beneath the northeast Japan arc. Geophys. Res. Lett. 27 (3), 425–428.

Iyer, H.M., 1992. Seismological detection and delineation of magma chambers: present status with emphasis on the western USA. In: Gasparini, P., Scarpa, R., Aki, K. (Eds.), Volcanic Seismology. Springer-Verlag, Berlin, pp. 299–338.

Iyer, H.M., Dawson, P.B., 1993. Imaging volcanoes using teleseismic tomography. In: Iyer, H.M., Hirahara, K. (Eds.), Seismic Tomography: Theory and Practice. Chapman and Hall, London.

Iyer, H.M., et al., 1981. A deep low-velocity body under the Yellowstone caldera, Wyoming: delineation using teleseismic P-wave residuals and tectonic interpretation. Geol. Soc. Am. Bull. 92 (Part I), 792–798.

Iyer, H.M., Hirahara, K. (Eds.), 1993. Seismic Tomography: Theory and Practice. Chapman and Hall.

Johnston, D.H., Toksoz, M.N., Timur, A., 1979. Attenuation of seismic waves in dry and saturated rocks: 2. Mechanisms. Geophysics 44, 691–711.

Kampfmann, W., Berckhemer, H., 1985. High temperature experiments on the elastic and anelastic behavior of magmatic rocks. Phys. Earth Planet. Inter. 40, 223–247.

Krastel, S., Schmincke, H.-U., 2002. Crustal structure of northern Gran Canaria, Canary Islands, deduced from active seismic tomography. J. Volcanol. Geotherm. Res. 115 (1–2), 153–177.

Laigle, M., Hirn, A., 1999. Explosion-seismic tomography of a magmatic body beneath Mount Etna; volatile discharge and tectonic control of volcanism. Geophys. Res. Lett. 26 (17), 2665–2668.

Lees, J.M., 1992. The magma system of Mount St. Helens: non-linear high resolution P-wave tomography. J. Volcanol. Geotherm. Res. 53 (1–4), 103–116.

Lees, J.M., Crosson, R.S., 1989. Tomographic inversion for three-dimensional velocity structure at Mount St. Helens using earthquake data. J. Geophys. Res. 94 (B5), 5716–5728.

Lees, J.M., Crosson, R.S., 1990. Tomographic imaging of local earthquake delay times for 3-D velocity variation in western Washington. J. Geophys. Res. 95 (B4), 4763–4776.

Lees, J.M., Crosson, R.S., 1991. Bayesian ART versus conjugate gradient methods in tomographic seismic imaging: an application at Mount St. Helens, Washington. In: Possolo, A. (Ed.), Spatial Statistics and Imaging. IMS Lecture Notes— Monograph Series. Inst. of Math. Statistics, Hayward, CA, pp. 186–208.

Lees, J.M., Lindley, G.T., 1994. Three-dimensional attenuation tomography at Loma Prieta: inverting t* for Q. J. Geophys. Res. 99 (B4), 6843–6863.

Lees, J.M., Ukawa, M., 1992. The South Fossa Magna, Japan, revealed by high resolution P and S-wave travel time tomography. Tectonophysics 207, 377–396.

Lees, J.M., Wu, H., 1999. P-wave anisotropy, stress, and crack distribution at Coso Geothermal Field, California. J. Geophys. Res. 104 (8), 17,955–17,973.

Lees, J.M., Wu, H., 2000. Poisson's ratio and porosity at Coso Geothermal Area, California. J. Volcanol. Geotherm. Res. 95, 157–173.

Lees, J.M., Symons, N., Chubarova, O., Gorelchik, V. and Ozerov, A., in press. Tomographic Images of Kliuchevskoi Volcano P-wave Velocity. In: Eichelberger, J., Izbekov, P., Kasahara, M., Lees J., Gordeev E. (Eds.), Volcanism and Tectonics of the Kamchatka Peninsula and Adjacent Arcs. AGU Monograph.

Londoño, J.M., Sudo, Y., 2003. Velocity structure and a seismic model for Nevado del Ruiz Volcano (Colombia). J. Volcanol. Geotherm. Res. 119 (1–4), 61–87.

Lutter, W.J., et al., 1995. Teleseismic P-wave image of crust and upper mantle structure beneath the Valles Caldera, New Mexico; initial results from the 1993 JTEX passive array. Geophys. Res. Lett. 22 (4), 505–508.

Masturyono, et al., 2001. Distribution of magma beneath Toba Caldera, North Sumatra, Indonesia, constrained by 3-dimensional P-wave velocities, seismicity, and gravity data. Geochem. Geophys. Geosyst. 2 (4). doi:10.1029/2000GC000096.

Mavko, G., Mukerji, T., Dvorkin, J., 1998. The Rock Physics Handbook: Tools for Seismic Analysis in Porous Media. Cambridge University Press, New York. 329 pp.

Mavko, G.M., 1980. Velocity and attenuation in partially molten rocks. J. Geophys. Res. 85 (B10), 5173–5189.

Mavko, G.M., Nur, A., 1978. Wave attenuation in partially saturated rocks. Geophysics 44, 161–178.

Menke, W., Levin, V., Sethi, R., 1995. Seismic attenuation in the crust at the mid-Atlantic boundary in south-west Iceland. Geophys. J. Int. 122, 175–185.

Menke, W., West, M., Tolstoy, M., 2002. Shallow-crustal magma chamber beneath the axial high of the CoAxial Segment of Juan de Fuca Ridge at the source site of the 1993 eruption. Geology 30 (4), 359–362.

Miller, D.S., Smith, R.B., 1999. P and S velocity structure of the Yellowstone volcanic field from local earthquake and controlled-source tomography. J. Geophys. Res. 104 (7), 15,105–15,121.

Mizutani, H., Kanamori, H., 1964. Variation of elastic wave velocity and attenuation property near melting temperature. J. Phys. Earth 12, 43–49.

Molina, I., Kumagai, H., Le Pennec, J.L., Hall, M., 2005. Three-dimensional P-wave velocity structure of Tungurahua Volcano, Ecuador. J. Volcanol. Geotherm. Res. 147 (1–2), 144–156.

Moran, S.C., Lees, J.M., Malone, S.D., 1999. P-wave velocity structure in the greater Mount Rainier area from local earthquake tomography. J. Geophys. Res. 104 (10), 10,775–10,786.

Mori, J.J., Eberhart-Phillips, D., Harlow, D.H., 1996. Three-dimensional velocity structure at Mount Pinatubo; resolving magma bodies and earthquake hypocenters. In: Newhall, C.G.e., Punongbayan, R.S.e. (Eds.), Fire and Mud; Eruptions and Lahars of Mount Pinatubo, Philippines, pp. 371–382.

Nakajima, J., Hasegawa, A., 2003. Tomographic imaging of seismic velocity structure in and around the Onikobe volcanic area, Northeastern Japan; implications for fluid distribution. J. Volcanol. Geotherm. Res. 127 (1–2), 1–18.

Nakamichi, H., 2005. 3D Velocity Structure of Mt. Fuji and the South Fossa Magna, Japan, Eos (Trans. AGU). p. T43A–1361.

Nakamichi, H., Ukawa, M., Sakai, S.i., 2004. Precise hypocenter locations of midcrustal low-frequency earthquakes beneath Mt. Fuji, Japan. Earth Planets Space 56 (12), e37–e40.

Nicholson, C., Simpson, D.W., 1985. Changes in Vp/Vs with depth: Implication for appropriate velocity models, improved earthquake locations, and material properties of the upper crust. Bull. Seismol. Soc. Am. 75, 1105–1124.

Nur, A., Simmons, G., 1969. The effect of saturation on velocity in low porosity rocks. Earth Planet. Sci. Lett. 7, 183–193.

O'Doherty, K.B., Bean, C.J., McCloskey, J., 1997. Coda wave imaging of the Long Valley Caldera using a spatial stacking technique. Geophys. Res. Lett. 24 (13), 1547–1550.

Ohmi, S., Lees, J.M., 1995. Three-dimensional P and S-wave velocity structure below Unzen Volcano. J. Volcanol. Geotherm. Res. 65, 1–26.

Okubo, P.G., Benz, H.M., Chouet, B.A., 1997. Imaging the crustal magma sources beneath Mauna Loa and Kilauea volcanoes, Hawaii. Geology 25 (10), 867–870.

Ozerov, A.Y., 2000. The evolution of high-alumina basalts of the Klyuchevskoy Volcano, Kamchatka, Russia, based on microprobe analyses of mineral inclusions. J. Volcanol. Geotherm. Res. 95, 65–79.

Pallister, J.S., Hoblitt, R.P., Crandell, D.R., Mullineaux, D.R., 1992. Mount St. Helens a decade after the 1980 eruptions: magmatic models, chemical cycles, and a revised hazards assessment. Bull. Volcanol. 54, 126–146.

Peppin, W.A., 1985. New evidence for magma bodies south of Long Valley Caldera, Mammoth Lakes, California. Eos, Trans. - Am. Geophys. Union 66 (46), 959.

Ritter, J.R.R., Evans, J.R., 1997. Deep structure of Medicine Lake Volcano, California. In: Fuchs, K., Altherr, R., Mueller, B., Prodehl, C. (Eds.), Tectonophysics. Elsevier, Amsterdam, pp. 221–241.

Rowan, L.R., Clayton, R.W., 1993. The three-dimensional structure of Kilauea Volcano, Hawaii, from travel time tomography. J. Geophys. Res. 98 (3), 4355–4375.

Sanders, C.O., 1993a. Local earthquake tomography; attenuation; theory and results. In: Iyer, H.M., Hirahara, K. (Eds.), Seismic Tomography: Theory and Practice. Chapman and Hall, London.

Sanders, C.O., 1993b. Reanalysis of S-to-P amplitude ratios for gross attenuation structure, Long Valley Caldera, California. J. Geophys. Res. 98 (12), 22,069–22,079.

Sanders, C.O., Ponko, S.C., Nixon, L.D., Schwartz, E.A., 1995. Seismological evidence for magmatic and hydrothermal structure in Long Valley caldera from local earthquake attenuation and velocity tomography. J. Geophys. Res. 100 (5), 8311–8326.

Sanders, C.O., Ponko, S.C., Nixon, L.D., Schwartz, E.A., Anonymous, 1994. Local earthquake attenuation and velocity tomography for magmatic and hydrothermal structure in Long Valley Caldera, California, Seismol. Res. Lett. 56.

Sato, H., Sacks, I.S., Murase, T., 1989. The use of laboratory velocity data for estimating temperature and partial melt fraction in the low velocity zone: comparison with heat flow and electrical conductivity studies. J. Geophys. Res. 94, 5689–5704.

Schurr, B., Asch, G., Rietbrock, A., Trumbull, R., Haberland, C., 2003. Complex patterns of fluid and melt transport in the central Andean subduction zone revealed by attenuation tomography. Earth Planet. Sci. Lett. 215 (1–2), 105–119.

Sherburn, S., Bannister, S., Bibby, H., 2003. Seismic velocity structure of the central Taupo volcanic zone, New Zealand, from local earthquake tomography. J. Volcanol. Geotherm. Res. 122 (1–2), 69–88.

Skinner, B.J., Porter, S.C., 2004. The Dynamic Earth: an Introduction to Physical Geology. Wiley, New York. 648 pp.

Soosalu, H., Einarsson, P., 2004. Seismic constraints on magma chambers at Hekla and Torfajökull volcanoes, Iceland Bull. Volcanol 66 (3), 276–286. doi:10.1007/s00445-003-0310-1.

Stauber, D.A., Green, S.M., Iyer, H.M., 1988. Three-dimensional P velocity structure if the crust below Newberry volcano, Oregon. J. Geophys. Res. 93 (B9), 10,095–10,107.

Steck, L.K., 1995. Simulated annealing inversion of teleseismic P-wave slowness and azimuth for crustal velocity structure at Long Valley Caldera. Geophys. Res. Lett. 22 (4), 497–500.

Stocker, R.L., Gordon, R.B., 1975. Velocity and internal friction in partial melts. J. Geophys. Res. 80, 4828–4836.

Takei, Y., 1998. Constituuitive mechanical relations of solid–liquid composites in terms of grain-boundary contiuity. J. Geophys. Res. 103, 18183–18203.

Tanaka, S., et al., 2002. Three-dimensional P-wave velocity structure of Iwate Volcano, Japan from active seismic survey. Geophys. Res. Lett. 29 (no.10, 4.).

Thurber, C.H., 1984. Seismic detection of the summit magma complex of Kilauea volcano, Hawaii. Science 233, 165–167.

Thurber, C.H., 1993. Local earthquake tomography; velocities and V (sub p) V (sub s); theory. In: Iyer, H.M., Hirahara, K. (Eds.), Seismic Tomography: Theory and Practice. Chapman and Hall, London.

Toksoz, M.N., Cheng, C.H., Aytekin, T., 1976. Velocities of seismic waves in porous rock. Geophysics 41, 621–645.

Tomatsu, T., Kumagai, H., Dawson, P.B., 2001. Tomographic inversion of P-wave velocity and Q structures beneath the Kirishima volcanic complex, southern Japan, based on finite difference calculations of complex traveltimes. Geophys. J. Int. 146 (3), 781–794.

Toomey, D.R., Foulger, G.R., 1989. Tomographic inversion of local earthquake data from the Hengill–Grensdalur central volcano complex, Iceland. J. Geophys. Res. 94 (12), 497–517.

Toomey, D.R., Purdy, G.M., Solomon, S.C., Wilcock, W.S.D., 1990. The three-dimensional seismic velocity structure of the east Pacific Rise near latitude 9°30′ N. Nature 347 (6294), 639–645.

Tryggvason, K., Husebye, E.S., Stefansson, R., 1983. Seismic image of the hypothesized Icelandic hot spot. Tectonophysics 100, 97–118.

Tsumura, A., 1995. Simultaneous estimation of attenuation structure, source parameters and site response spectra: application to the northeastern part of Honshu, Japan. Ph.D. Thesis, Tohoku University, Sendai, Japan.

Tsumura, N., Matsumoto, S., Horiuchi, S., Hasegawa, A., 2000. Three-dimensional attenuation structure beneath the northeastern Japan arc estimated from spectra of small earthquakes. Tectonophysics 319 (4), 241–260.

Vanorio, T., Virieux, J., Capuano, P., Russo, G., 2005. Three-dimensional seismic tomography from P waves and S wave microearthquake travel times and rock physics characterization of the Campi Flegrei Caldera. J. Geophys. Res. 110 (no.B3, 14.).

Villasenor, A., et al., 1998. Three-dimensional P wave velocity structure of Mt. Etna, Italy. Geophys. Res. Lett. 25 (11), 1975–1978.

Walck, M.C., 1988. Three-dimensional variations in shear structure and Vp/Vs for the Coso region, California. J. Geophys. Res. 93, 2047–2052.

Weiland, C.M., Steck, L.K., Dawson, P.B., Korneev, V.A., 1995. Nonlinear teleseismic tomography at Long Valley Caldera, using three-dimensional minimum travel time ray tracing. J. Geophys. Res. 100 (10), 20,379–20,390.

Winkler, K., Nur, A., 1979. Pore fluids and seismic attenuation in rocks. Geophys. Res. Lett. 6, 1–4.

Wu, H., Lees, J.M., 1996. Attenuation structure of the Coso Geothermal area, California, from pulse width data of P-wave. Bull. Seismol. Soc. Am. 86, 1574–1590.

Wu, H., Lees, J.M., 1999. Three-dimensional P and S wave velocity structures of the Coso Geothermal Area, California, from microseismic traveltime data. J. Geophys. Res. 104:, 13,217–13,233.

Yamamoto, K., Ida, Y., 1994. Three-dimensional P-wave velocity structure of Kirishima voclanoes using regional seismic events (in Japanese). Bull. Earthq. Res. Inst. Univ. Tokyo 69, 267–289.

Yuan, H., Dueker, K., 2005. Teleseismic P-wave tomogram of the Yellowstone plume. Geophys. Res. Lett. 32 (7), 4. doi:10.1029/2004GL022056.

Zhao, D., Hasegawa, A., 1993. P wave tomographic imaging of the crust and upper mantle beneath the Japan Islands. J. Geophys. Res. 98 (3), 4333–4353.

Zhao, D., Hasegawa, A., Kanamori, H., 1994. Deep structure of Japan subduction zone as derived from local, regional, and teleseismic events. J. Geophys. Res. 99 (11), 22,313–22,329.

Zhao, D., Mishra, O.P., Sanda, R., 2002. Influence of fluids and magma on earthquakes; seismological evidence. Phys. Earth Planet. Inter. 132 (4), 249–267.

Zhao, D., et al., 1997. Depth extent of the Lau back-arc spreading center and its relation to subduction processes. Science 278 (5336), 254–257.

Zollo, A., et al., 1998. An image of Mt. Vesuvius obtained by 2D seismic tomography. In: Spera, F.J., de Vivo, B., Ayuso, R.A., Belkin, H.E. (Eds.), J. Volcanol. Geotherm. Res. , pp. 161–173.

Zollo, A., et al., 2003. Evidence for the buried rim of Campi Flegrei Caldera from 3-d active seismic imaging. Geophys. Res. Lett. 30 (no.19, 4.).